ACS OMEGA

http://pubs.acs.org/journal/acsodf

Article

Modeling the Inhibition Kinetics of Curcumin, Orange G, and Resveratrol with Amyloid-β Peptide

Chandra Mouli R. Madhuranthakam,* Arash Shakeri, and Praveen P. N. Rao*

Cite This: *ACS Omega* 2021, 6, 8680−8686

Read Online

ACCESS | Metrics & More | Article Recommendations

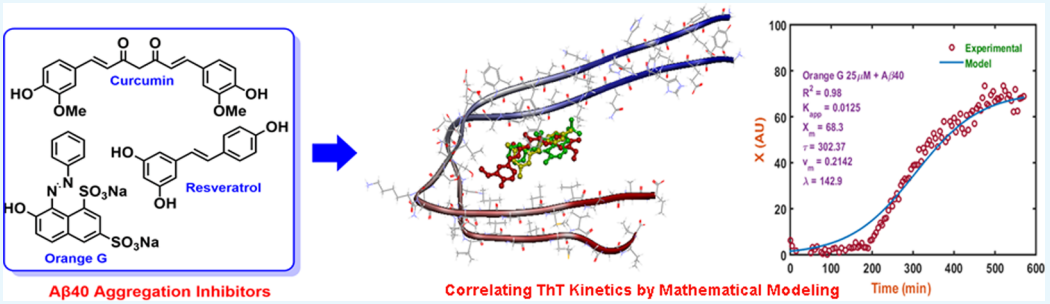

ABSTRACT: The β-amyloid (Aβ) protein aggregation into toxic forms is one of the major factors in the Alzheimer's disease (AD) pathology. Screening compound libraries as inhibitors of Aβ-aggregation is a common strategy to discover novel molecules as potential therapeutics in AD. In this regard, thioflavin T (ThT)-based fluorescence spectroscopy is a widely used in vitro method to identify inhibitors of Aβ aggregation. However, conventional data processing of the ThT assay experimental results generally provides only qualitative output and lacks inhibitor-specific quantitative data, which can offer a number of advantages such as identification of critical inhibitor-specific parameters required to design superior inhibitors and reduce the need to conduct extensive in vitro kinetic studies. Therefore, we carried out mathematical modeling based on logistic equation and power law (PL) model to correlate the experimental results obtained from the ThT-based Aβ40 aggregation kinetics for small-molecule inhibitors curcumin, orange G, and resveratrol and quantitatively fit the data in a logistic equation. This approach provides important inhibitor-specific parameters such as lag time λ, inflection point τ, maximum slope v_m, and apparent rate constant k_{app}, which are particularly useful in comparing the effectiveness of potential Aβ40 aggregation inhibitors and can be applied in drug discovery campaigns to compare and contrast Aβ40 inhibition data for large compound libraries.

INTRODUCTION

Amyloid proteins are implicated in a number of diseases including Alzheimer's disease (AD), Parkinson's disease (PD), prion disease, and so on.[1,2] These diseases are characterized by the misfolding and aggregation of proteins such as amyloid-β (Aβ), α-synuclein and prion proteins into toxic β-sheet-rich species.[3−5] To develop potential therapeutics for these diseases, preventing the misfolding and aggregation of amyloid proteins is considered as an attractive strategy. Several studies have reported the design of novel molecules capable of inhibiting or minimizing amyloid protein aggregation.[6−10]

In AD, Aβ40 and Aβ42 peptides are known to undergo misfolding and aggregation to form neurotoxic species.[11,12] Consequently decreasing the accumulation of these neurotoxic peptides is known to provide cognitive benefits in AD.[13−16] Considering the potential therapeutic applications of Aβ aggregation inhibitors, it is critical to understand the molecular mechanisms of Aβ aggregation to develop novel therapies for AD. In this regard, the kinetics of Aβ aggregation has been studied experimentally using fluorescent probes such as thioflavin T (ThT) and other dyes.[17−20] These studies have helped in understanding the molecular processes involved in Aβ aggregation. In vitro experiments have shown that the Aβ aggregation process exhibits a sigmoidal curve, where Aβ monomer gets converted to higher-order aggregates including dimers, trimers, oligomers, protofibrils, and fibrils.[21−25] This time-dependent transition of Aβ monomer into higher-order aggregates is represented by the initial lag phase, subsequent rapid growth phase, followed by the saturation phase to give the sigmoidal curve. Studies have also demonstrated that in vivo, Aβ undergoes sigmoidal growth kinetics.[26] This evidence suggests that investigating the Aβ-aggregation kinetics, by applying the principles of mathematical modeling, and

Received: February 2, 2021
Accepted: March 9, 2021
Published: March 19, 2021

correlating the outcomes to the experimental inhibition of Aβ aggregation, in the presence of Aβ aggregation inhibitors, can be used as a powerful tool to (i) understand the complex mechanisms of Aβ aggregation and (ii) to predict the antiaggregation activity of potential inhibitors. In this context, Michaels and co-workers have developed elegant chemical reaction kinetics based on mathematical modeling, to understand and study Aβ aggregation mechanisms using experimental measurements based on growth kinetics.[25] The workflow includes (i) a differential rate law that provides the rates of formation of various Aβ species as a function of time, (ii) an integrated rate law that provides concentrations of Aβ species as a function of time, and (iii) global curve fitting of the experimental kinetic data obtained with the integrated rate laws, to understand the mechanisms.[23,24] Other models proposed to study drug dosage response includes the probit, Weibull, and the all-hit-multi-target (AHMT) models.[1,2] For example, Rial and co-workers used the Weibull distribution model instead of the power law (PL) Model, to study the effect of heavy metals on bacterial growth.[27] Peppas and Narasimhan[28] described the importance of establishing mathematical models in the drug-delivery/release processes, where the models and their parameters can lead to an advanced analysis of the system being modeled. In another interesting study, a recent work used bivariate sigmoidal equation, to model Aβ aggregation kinetics and their inhibition by small molecules.[29] Therefore, developing mathematical modeling to study the inhibitory effects of known Aβ-aggregation inhibitors can help in understanding the mechanisms of aggregation and predict the inhibitory profiles of unknown compound libraries, without the need to conduct extensive experiments, which has the potential to reduce the time and cost involved in compound screening during drug discovery efforts. We used a bivariate mathematical model using a logistic equation based on autocatalytic origin in combination with a PL model for the compound concentration, to describe the Aβ40 growth inhibition kinetics of curcumin, orange G, and resveratrol (Figure 1).[7,29] These

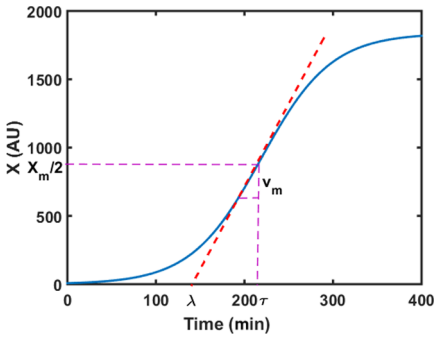

Figure 1. Typical response of the logistic equation and graphical representation of the parameters (λ, τ, v_m, and X_m).

small molecules are known to bind between the β-sheet assembly parallel to the fiber axis and prevent Aβ40 fibrillogenesis.[4,30] The Aβ40 growth kinetics was monitored at various concentrations for the three inhibitors using the ThT-based fluorescence studies. These investigations show that mathematical modeling of Aβ40 aggregation kinetics can be used as a valuable tool to study the mechanisms of small-molecule inhibitors by calculating a number of parameters such as lag time λ, inflection point τ, maximum slope v_m, and apparent rate constant k_{app} for compound libraries, which can assist in (i) comparing the efficiency of Aβ40 aggregation inhibitors, (ii) identifying promising leads for further experimental analysis, and (iii) minimizing the need to conduct extensive kinetic experiments.

MATERIALS AND METHODS

Thioflavin T-Based Aβ40 Kinetics Assay. The known Aβ40 aggregation inhibitors curcumin, orange G, and resveratrol were obtained from Sigma-Aldrich, Oakville, Canada, and Cayman Chemical Company, Ann Arbor, and were >95% pure. The Aβ40 peptide in the form of hexafluoro-2-propanol (HFIP) film was obtained from rPeptide, Georgia, and was >97% pure. The aggregation kinetics assay was carried out using thioflavin T (ThT)-based fluorescence spectroscopy.[17,19,31] The Aβ40 stock solution (1 mg/mL) was prepared first by adding 1% NH_4OH solution and was diluted further to obtain 500 μM solution in phosphate buffer (pH 8.0). Curcumin, orange G, and resveratrol stock solutions (10 000 μM) were prepared in DMSO, diluted in phosphate buffer (pH 8.0), and were sonicated for 30 min. The final DMSO concentration per well was 1% v/v or lower. The ThT fluorescent dye stock solution (15 μM) was prepared in 50 mM glycine buffer (pH 8.5), and the aggregation kinetics assay was carried out using a Corning 384-well flat, clear-bottom black plate with each well containing 44 μL of ThT, 20 μL of phosphate buffer (pH 8.0), 8 μL of curcumin, orange G, or resveratrol at different concentrations (1, 5, 10, and 25 μM), and 8 μL of Aβ40 (5 μM). The microplate was incubated at 37 °C with a plate cover, under shaking, and the fluorescence intensity was measured every 5 min using a SpectraMax M5 multimode plate reader (excitation = 440 nm and emission = 490 nm), over a period of 24 h. Appropriate control experiments that contain Aβ40 and buffer alone, and compounds alone, at different concentrations were kept to monitor any interference in the fluorescence intensity measurements. The percentage inhibition was calculated using the equation 100% control − [(IF_i − IF_o)], where 100% control indicates no inhibitor and IF_i and IF_o are the fluorescence intensities in the presence and absence of ThT, respectively. These control readings assist in accounting for potential interference by test compounds by ThT fluorescence quenching.[32] The results were expressed as percentage inhibition of three separate experiments in triplicate measurements (n = 3).

Mathematical Modeling. The aggregation of Aβ40 peptide alone or the control group and in the presence of curcumin, orange G, and resveratrol was modeled using the logistic equation, which is a differential equation based on the known autocatalytic reaction.[7] This model is given by eq 1.

$$\frac{dX}{dt} = k_{app}X\left(1 - \frac{X}{X_m}\right) \quad (1)$$

where X is the fluorescence intensity of the Aβ peptide, which is an indirect measure of aggregation growth, k_{app} is the apparent rate constant (also called as specific rate constant), X_m is the fluorescence intensity corresponding to maximum aggregation growth, and t is the time (Figure 1).[29] Equation 1 can be integrated using the initial condition at time t = 0, X = X_0, where X_0 is the fluorescence intensity corresponding to the initial aggregation growth. An explicit form for the solution of

https://doi.org/10.1021/acsomega.1c00610
ACS Omega 2021, 6, 8680−8686

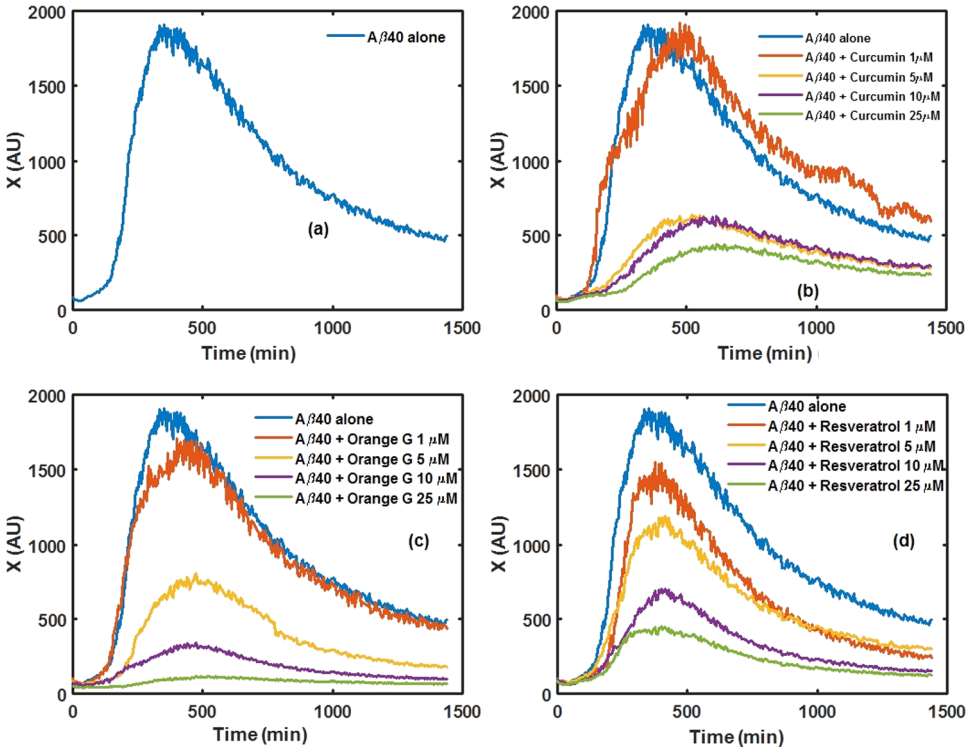

Figure 2. ThT fluorescence intensity vs time for (a) Aβ40 alone (5 μM), (b) curcumin, (c) orange G, and (d) resveratrol at concentrations 1, 5, 10, and 25 μM in the presence of Aβ40 (5 μM) in phosphate buffer 37 °C at pH 8.0 (excitation = 440 nm; emission = 490 nm). The results are based on three independent experiments (n = 3).

model as per eq 1 is given by eq 2, where X is obtained as a function of k_{app}, X_m, and X_0.[29]

$$X = \frac{X_m}{1 + \exp\left[\ln\left(\frac{X_m - X_0}{X_0} - k_{app}\cdot t\right)\right]} \quad (2)$$

A typical response curve for X vs t is shown in Figure 1. Some of the important parameters that characterize Aβ40 aggregation are obtained by estimating the lag phase (λ), the maximum slope (ν_m), and the corresponding time at the inflection point (τ), also referred to as the half-maximal fluorescence time point (t_{50}). These parameters are very important in assessing the performance of compounds (curcumin, orange G, and resveratrol) with respect to the inhibition of Aβ40 aggregation. The time corresponding to inflection point, τ, can be obtained by equating the derivative in eq 1 to zero, or it can also be obtained by substituting $X = X_m/2$ in eq 2, as it represents the time required to obtain semimaximum fibrillation growth. The corresponding expression for τ is given by eq 3.

$$\tau = \frac{1}{k_{app}} \ln\left(\frac{X_m - X_0}{X_0}\right) \quad (3)$$

The slope at the inflection point, ν_m, was obtained by evaluating the derivative dX/dt at time $t = \tau$ using eq 2, and the lag time λ was obtained using the definition of slope ($\Delta X/\Delta t$). Using these definitions, eqs 4 and 5 were obtained for calculating ν_m and λ in terms of known parameters (such as X_m, τ, and k_{app}).

$$\nu_m = \frac{X_m k_{app}}{4} \quad (4)$$

$$\lambda = \tau - \frac{2}{k_{app}} \quad (5)$$

RESULTS AND DISCUSSION

Thioflavin T-Based Aβ40 Kinetics Assay. The aggregation kinetic studies for Aβ40 alone show the typical sigmoidal curve with a short lag phase, followed by a rapid growth phase and an elongation phase in a 24 h period (Figure 2a).[22,31] Under our assay conditions, the saturation phase tends to see a gradual decline in the ThT fluorescence intensity for the growth kinetics of Aβ40 alone. Curcumin is a hydrophobic polyphenol derived from the herb *Curcuma longa* and is known to prevent Aβ aggregation.[33] The results from the ThT aggregation kinetics for Aβ40 in the presence of curcumin clearly show its antiaggregation properties. At 1 μM, curcumin did not show inhibition, and as its concentration was increased to 5, 10, and 25 μM (Figure 2b), there was a concentration-dependent decline in the fluorescence intensity and the Aβ40 aggregation inhibition percent ranged from 40 to 52% at 24 h time point. Figure 2c shows the aggregation kinetics data for orange G, which is a synthetic compound with known Aβ-aggregation inhibition properties.[30] Similar to curcumin, at a lower concentration (1 μM), orange G did not show inhibition; however, at increased concentrations, it exhibited superior inhibition (63−86% range at 24 h time point) compared to curcumin. The phenolic antioxidant resveratrol (*trans*-3,4′,5-trihydroxystilbene), another natural compound known to inhibit Aβ aggregation,[34,35] exhibited antiaggregation properties (38−75% inhibition of Aβ40 aggregation at 24 h time point) at all of the tested concentrations as shown in Figure 2d, although it was not as potent as orange G.

https://doi.org/10.1021/acsomega.1c00610
ACS Omega 2021, 6, 8680−8686

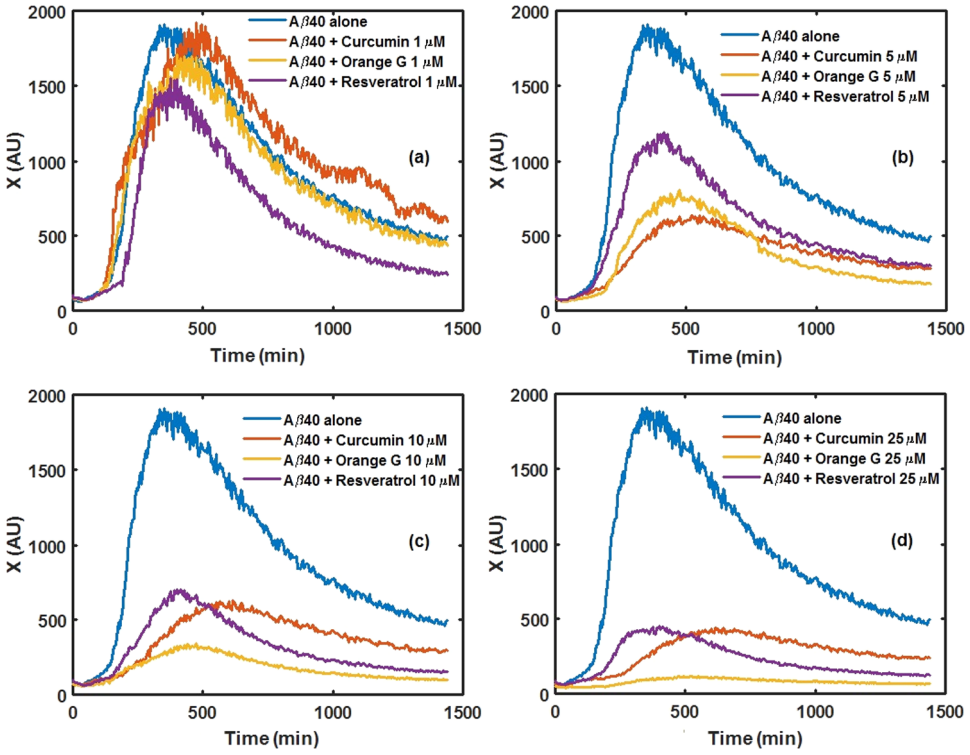

Figure 3. Comparison of the ThT fluorescence intensities of curcumin, orange G, and resveratrol at concentrations of (a) 1 μM, (b) 5 μM, (c) 10 μM, and (d) 25 μM in the presence of Aβ40 (5 μM) in phosphate buffer 37 °C at pH 8.0 (excitation = 440 nm; emission = 490 nm). The results are based on three independent experiments (n = 3).

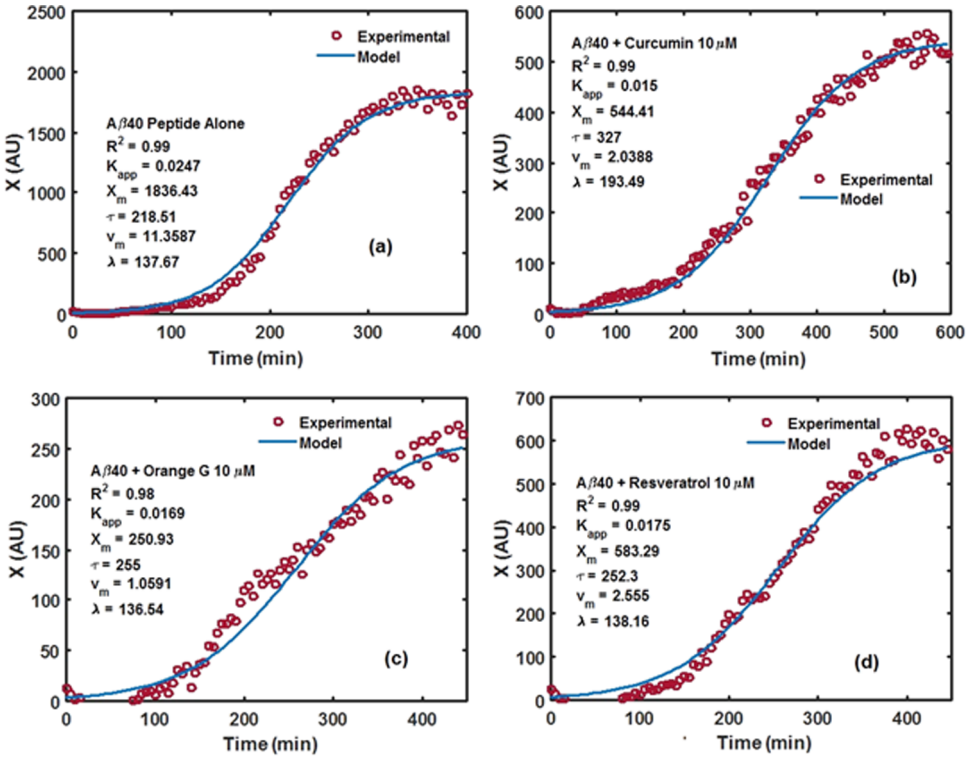

Figure 4. Comparison of fluorescence intensity (X) and time obtained from the fitted model and the experimental data for (a) Aβ40 alone, (b) Aβ40 and curcumin at 10 μM, (c) Aβ40 and orange G at 10 μM, and (d) Aβ40 and resveratrol at 10 μM.

Figure 3a–d shows the comparison of the anti-Aβ aggregation properties of curcumin, orange G, and resveratrol at 1, 5, 10, and 25 μM, respectively. It also shows that both curcumin and orange G were able to extend the lag phase at 5 μM (Figure 3b), and as the concentration was increased to 10 and 25 μM, all of the three compounds were able to extend the

https://doi.org/10.1021/acsomega.1c00610
ACS Omega 2021, 6, 8680−8686

Table 1. Mathematical Modeling Parameters for Aβ40 Aggregation Inhibition by Curcumin

		Concentration of curcumin in μM			
Parameters	Aβ40 peptide alone	1	5	10	25
R^2	0.99	0.94	1.00	0.99	0.99
k_{app} (min^{-1})	0.0253	0.0205	0.0167	0.0150	0.0126
X_m (AU)	1836.71	1791.76	561.75	544.41	375.98τ
τ (min)	218.73	234.47	284.22	327.00	350.80
v_m (AU/min)	11.5967	9.1777	2.3444	2.0388	1.1839
λ (min)	139.54	136.85	164.41	193.49	192.01

Table 2. Mathematical Modeling Parameters for Aβ40 Aggregation Inhibition by Orange G and Resveratrol

	Concentration of orange G in μM				Concentration of resveratrol in μM			
Parameters	1	5	10	25	1	5	10	25
R^2	0.98	0.99	0.98	0.98	0.98	0.99	0.99	0.99
k_{app} (min^{-1})	0.0254	0.0194	0.0169	0.0125	0.022	0.0274	0.0176	0.0214
X_m (AU)	1623.76	713.46	250.93	68.30	1353.34	1076.15	527.60	357.32
τ (min)	218.53	274.39	255.00	302.37	246.95	237.95	245.28	218.46
v_m (AU/min)	10.3021	3.4550	1.0591	0.2142	7.4581	7.3816	2.3226	1.9114
λ (min)	139.72	171.14	136.54	142.90	156.22	165.05	131.70	124.99

lag phase duration (Figure 3c,d). This study also shows that orange G is a very effective inhibitor of Aβ40 aggregation at higher concentrations compared to curcumin or resveratrol.

Mathematical Modeling. To quantitatively assess the obtained results, the Aβ40 growth kinetics experimental data for the control and in the presence of different concentrations of Aβ40 aggregation inhibitors curcumin, orange G, and resveratrol were modeled using the kinetics equation that describes the fluorescence intensity as a measure of Aβ fibrillogenesis during the experimental run period. The mathematical modeling was based on the assumptions that compounds screened (i) are not promoters of Aβ40 aggregation; (ii) exhibit noncovalent binding; and (iii) are small molecules. The fluorescence intensities obtained from these experiments were fitted with the logistic equation described earlier (eq 1). The parameters k_{app} and X_m were estimated using a nonlinear least-squares fit where the ordinary differential equation (ODE) with the corresponding initial condition ($X = X_0$ at $t = 0$) was also solved simultaneously. A program in MATLAB (Version R2020b) with a built-in function lsqcurvefit.m was used for the curve fitting and ode45.m was used for solving the ODE. In all simulations, the initial condition in ODE described in eq 1 was modified such that at $t = 0$, $X = 0$. This was done so that the parameters such as X_m can be compared across the different concentration range for the inhibitors used in this study. The logistic equation fits well for all scenarios considered in this study such as different inhibitors, at different concentrations. The degree of goodness of fit was quantified using the correlation coefficient R^2. The R^2 value in all of the scenarios considered was observed to be >0.95, which shows that the experimental results are in good agreement with the proposed logistic model. In all of the mathematical simulations, the apparent rate constant k_{app} was estimated using X_m and X_0 from the experimental results. Other important parameters such as τ, v_m, and λ, which are functions of k_{app}, X_m, and X_0 were calculated using eqs 3−5, respectively.

As an example, Figure 4a−d shows the comparison of the experimental results with the model fitted using eq 1 for Aβ40 alone and in the presence of inhibitors curcumin, orange G, and resveratrol at 10 μM. The corresponding parameters such as k_{app}, τ, v_m, and λ obtained from estimation and calculation based on eqs 3−5 are shown in Figure 4. Further, the effect of inhibitor concentration (C) on the parameters X_m, k_{app}, and λ for all of the inhibitors was modeled using a power law (PL) model as shown in eq 6. The logistic equation in combination with the PL model forms a comprehensive bivariate model that can be used to predict the effect of varying concentrations of different inhibitors on Aβ40 aggregation.

Tables 1 and 2 shows the summary of parameters obtained from the mathematical simulations for different inhibitors at different concentrations. From this, it is apparent that the k_{app} and X_m values decreased with an increase in the compound concentration for all of the three inhibitors. Interestingly, the lag time λ, which is an important compound-specific parameter, increased with increasing concentration of curcumin, while that was not the case for resveratrol, which exhibited reductions in lag time with increasing concentrations (5, 10, and 25 μM respectively). This highlights the value of using mathematical simulations to understand the inhibition mechanisms of Aβ aggregation inhibitors by calculating their lag time λ, which is not always possible by conventional data processing for ThT-based aggregation kinetics. Furthermore, analysis of v_m data for Aβ40 alone and in the presence of inhibitors clearly shows that effective Aβ40 aggregation inhibitors show a reduction in v_m values, which was directly dependent on the inhibitor concentration (Tables 1 and 2).

Among the different parameters obtained from the modeling of the experimental data, the fluorescence intensity corresponding to maximum aggregation growth (X_m) is of greater importance, as it can be used to calculate the effectiveness of aggregation inhibitors. The IC_{50} value is defined as the concentration of the inhibitor (curcumin, orange G, and resveratrol) that reduces the maximum fluorescence intensity of Aβ40 alone by 50%. A plot of X_m versus concentration shows that the obtained data can be conveniently modeled using a PL model described by the following equation.

$$X_m = k_1 C^{k_2} \quad (6)$$

where C is the compound concentration in μM, and k_1 and k_2 are the corresponding constants.

https://doi.org/10.1021/acsomega.1c00610
ACS Omega 2021, 6, 8680−8686

As an example, the PL model versus experimental fitting for X_m and concentration C for orange G was solved using eq 6 as shown in Figure 5. The values of k_1 and k_2 were obtained for

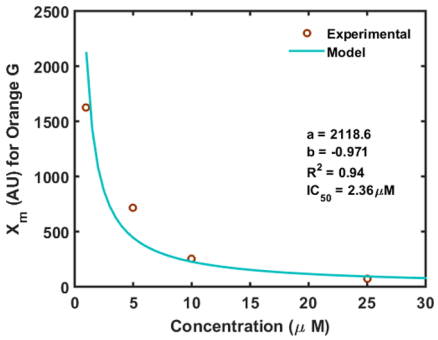

Figure 5. PL model versus experimental values for X_m versus concentration using orange G.

different concentrations of curcumin, orange G, and resveratrol using eq 6, as shown in Table 3. It clearly shows that the PL

Table 3. Using the PL Equation to Calculate the IC_{50} Values for Aβ40 Inhibitors

Inhibitor	R^2	k_1	k_2	IC_{50} in μM
Curcumin	0.96	1585.8	−0.480	3.11 ± 1.06
Orange G	0.94	2118.6	−0.971	2.63 ± 0.85
Resveratrol	0.83	1548.0	−0.426	3.39 ± 1.96

model is adequate to represent the relationship between X_m and the inhibitor concentration. This also shows the application of eq 6 in calculating the IC_{50} values of inhibitors, which is challenging for nonlinear outputs such as Aβ growth kinetics by conventional data processing. The calculated IC_{50} values for curcumin, orange G, and resveratrol (Table 3) show that orange G is a better inhibitor of Aβ40 aggregation (IC_{50} = 2.6 μM) compared to others (curcumin IC_{50} = 3.1 μM; resveratrol IC_{50} = 3.4 μM). Furthermore, if we compare the performances of these three inhibitors at lower concentrations, at 5 μM, curcumin demonstrates better inhibition than orange G and resveratrol based on X_m and lag time (λ) with lower values (Tables 1 and 2). The lag time λ in minutes is a strong function of k_{app}. This is in agreement with the smaller k_{app} values observed for curcumin compared to k_{app} values obtained for orange G and resveratrol (Tables 1 and 2) and demonstrates that apparent rate constant k_{app} is another important parameter, which can be calculated by mathematical simulation that together with lag time λ can be analyzed to design better Aβ40 aggregation inhibitors.

CONCLUSIONS

The antiaggregation properties of curcumin, orange G, and resveratrol toward Aβ40 aggregation were investigated by the ThT-based fluorescence aggregation kinetic study. These experiments showed that all of the three compounds exhibited significant inhibitory effects in reducing the Aβ40 fibrillogenesis in a concentration-dependent manner with orange G, exhibiting superior inhibition at higher concentrations compared to curcumin and resveratrol. The experimental data obtained were correlated by calculating a number of compound-related parameters by mathematical modeling using the bivariate model by combining the logistic equation and autocatalytic model. The mathematical modeling was used to estimate compound-specific parameters such as lag time (λ), maximum slope (ν_m), and the corresponding time at the inflection point (τ), which were correlated with the experimentally obtained fluorescence intensity (X_m) as a function of time. Interestingly, the bivariate model was able to highlight subtle differences in the antiaggregation properties of compounds, which is difficult to identify by conventional data processing. Parameters derived from the modeling such as lag time (λ) and k_{app} values further showed that curcumin was more effective at lower concentration compared to orange G and resveratrol. Furthermore, the PL model provides a simplified eq 6, to calculate IC_{50} values, which is not adequately addressed in the literature, for nonlinear outputs such as Aβ aggregation kinetics. The PL model is able to provide precise IC_{50} values using the experimental data, which assists in distinguishing better inhibitors from the aggregation inhibition screen. These studies demonstrate the application of bivariate modeling in correlating the experimental data to analyze the antiaggregation properties of inhibitors and have direct application in drug discovery campaigns[36] to identify and design novel Aβ aggregation inhibitors.

AUTHOR INFORMATION

Corresponding Authors

Chandra Mouli R. Madhuranthakam − *Chemical Engineering Department, Abu Dhabi University, Abu Dhabi, UAE*; orcid.org/0000-0001-7928-7128; Email: chandra.mouli@adu.ac.ae

Praveen P. N. Rao − *School of Pharmacy, Health Sciences Campus, University of Waterloo, Waterloo, Ontario N2L 3G1, Canada*; orcid.org/0000-0001-5703-8251; Email: praopera@uwaterloo.ca

Author

Arash Shakeri − *School of Pharmacy, Health Sciences Campus, University of Waterloo, Waterloo, Ontario N2L 3G1, Canada*

Complete contact information is available at: https://pubs.acs.org/10.1021/acsomega.1c00610

Notes

The authors declare no competing financial interest.

ACKNOWLEDGMENTS

The authors thank NSERC-Discovery (RGPIN: 038302014), Early Researcher Award (ERA), Ministry of Research, Innovation and Science, Government of Ontario, Canada, for financial support of this research project (P.P.N.R.); Ministry of Colleges and Universities, Government of Ontario, for Ontario Graduate Scholarship (A.S.); and Abu Dhabi University for collaborative research.

REFERENCES

(1) Chiti, F.; Dobson, C. M. Protein misfolding, amyloid formation, and human disease: A summary of progress over the last decade. *Annu. Rev. Biochem.* **2017**, *86*, 27−68.

(2) Ke, P. C.; Sani, M. A.; Ding, F.; Kakinen, A.; Javed, I.; Separovic, F.; Davis, T. P.; Mezzenga, R. Implications of peptide assemblies in amyloid diseases. *Chem. Soc. Rev.* **2017**, *46*, 6492−6531.

(3) Hamley, I. W. The amyloid beta peptide: A chemist's perspective. Role in Alzheimer's and fibrillation. *Chem. Rev.* **2012**, *112*, 5147−5192.

(4) Eisenberg, D. S.; Sawaya, M. R. Structural studies of amyloid proteins at the molecular level. *Annu. Rev. Biochem.* **2017**, *86*, 69−95.
(5) Scheckel, C.; Aguzzi, A. Prions, prionoids and protein misfolding disorders. *Nat. Rev. Genet.* **2018**, *19*, 405−418.
(6) Mohamed, T.; Shakeri, A.; Rao, P. N. P. Amyloid cascade in Alzheimer's disease: Recent advances in medicinal chemistry. *Eur. J. Med. Chem.* **2016**, *113*, 258−272.
(7) Sabaté, R.; Gallardo, M.; Estelrich, J. An autocatalytic reaction as a model for the kinetics of the aggregation of beta-amyloid. *Biopolymers* **2003**, *71*, 190−195.
(8) Young, L. M.; Ashcroft, A. E.; Radford, S. E. Small molecule probes of protein aggregation. *Curr. Opin. Chem. Biol.* **2017**, *39*, 90−99.
(9) Verwilst, P.; Kim, H. S.; Kim, S.; Kang, C.; Kim, J. S. Shedding light on tau protein aggregation: the progress in developing highly selective fluorophores. *Chem. Soc. Rev.* **2018**, *47*, 2249−2265.
(10) Pujols, J.; Pena-Diaz, S.; Lazaro, D. F.; Peccati, F.; Pinheiro, F.; Gonzales, D.; Carija, A.; Navarro, S.; Conde-Gimenez, M.; Garcia, J.; Guardiola, S.; Giralt, E.; Salvatella, X.; Sancho, J.; Sodupe, M.; Outeiro, T. F.; Dalfo, E.; Ventura, S. Small molecule inhibits synuclein aggregation, disrupts amyloid fibrils, and prevents degeneration of dopaminergic neurons. *Proc. Natl. Acad. Sci. U.S.A.* **2018**, *115*, 10481−10486.
(11) Pauwels, K.; Williams, T. L.; Morris, K. L.; Jonckheere, W.; Vandersteen, A.; Kelly, G.; Schymkowitz, J.; Rousseau, F.; Pastore, A.; Serpell, L. C.; Broersen, K. Structural basis for increased toxicity of pathological Aβ42:Aβ40 ratios in Alzheimer disease. *J. Biol. Chem.* **2012**, *287*, 5650−5660.
(12) Kayed, R.; Lasagna-Reeves, C. A. Molecular mechanisms of amyloid oligomers toxicity. *J. Alzheimer's Dis.* **2012**, *33*, S67−S78.
(13) Martikainen, I. K.; Kemppainen, N.; Johansson, J.; Teuho, J.; Helin, S.; Liu, Y.; Helisalmi, S.; Soininen, H.; Parkkola, R.; Ngandu, T.; Kivipelto, M.; Rinne, J. O. Brain β-amyloid and atrophy in individuals at increased risk of cognitive decline. *Am. J. Neuroradiol.* **2019**, *40*, 80−85.
(14) Xing, H. Y.; Li, B.; Peng, D.; Wang, C. Y.; Wang, G. Y.; Li, P.; Le, Y. Y.; Wang, J. M.; Ye, G.; Chen, J. H. A novel monoclonal antibody against the N-terminus of $A\beta_{1\text{-}42}$ reduces plaques and improves cognition in a mouse model of Alzheimer's disease. *PLoS One* **2017**, *12*, No. e0180076.
(15) Okamoto, M.; Gray, J. D.; Larson, C. S.; Kazim, S. F.; Soya, H.; McEwen, B. S.; Pereira, A. C. Riluzole reduces amyloid beta pathology, improves memory, and restores gene expression changes in a transgenic mouse model of early-onset Alzheimer's disease. *Transl. Psychiatry* **2018**, *8*, No. 153.
(16) Sevigny, J.; Chiao, P.; Bussiere, T.; Weinreb, P. H.; Williams, L.; Maier, M.; Dunstan, R.; Salloway, S.; Chen, T.; Ling, Y.; O'Gorman, J.; Qian, F.; Arastu, M.; Li, M.; Chollate, S.; Brennan, M. S.; Quintero-Monzon, O.; Scannevin, R. H.; Arnold, H. M.; Engber, T.; Rhodes, K.; Ferrero, J.; Hang, Y.; Mikulskis, A.; Grimm, J.; Hock, C.; Nitsch, R. M.; Sandrock, A. *Nature* **2016**, *537*, 50−56.
(17) LeVine, H. Quantification of beta-sheet amyloid fibril structures with thioflavin T. *Methods Enzymol.* **1999**, *309*, 274−284.
(18) Jameson, L. P.; Smith, N. W.; Dzyuba, S. V. Dye-binding assays for evaluation of the effects of small molecule inhibitors on amyloid (Aβ) self-assembly. *ACS Chem. Neurosci.* **2012**, *3*, 808−819.
(19) Xue, C.; Lin, T. Y.; Chang, D.; Guo, Z. Thioflavin T as an amyloid dye: fibril quantification, optimal concentration and effect on aggregation. *R. Soc. Open Sci.* **2017**, *4*, No. 160696.
(20) Rajasekhar, K.; Narayanaswamy, N.; Murugan, N. A.; Agren, H.; Govindaraju, T. A high affinity red fluorescence and colorimetric probe for amyloid β aggregates. *Sci. Rep.* **2016**, *6*, No. 23668.
(21) Burdick, D.; Soreghan, B.; Kwon, M.; Kosmoski, J.; Knauer, M.; Henschen, A.; Yates, J.; Cotman, C.; Glabe, C. Assembly and aggregation properties of synthetic Alzheimer's Aβ amyloid peptide analogs. *J. Biol. Chem.* **1992**, *267*, 546−554.
(22) Arosio, P.; Knowles, T. P. J.; Linse, S. On the lag phase in amyloid fibril formation. *Phys. Chem. Chem Phys.* **2015**, *17*, 7606−7618.
(23) Meisl, G.; Yang, X.; Hellstrand, E.; Frohm, B.; Kirkegaard, J. B.; Cohen, S. I.; Dobson, M.; Linse, S.; Knowles, T. P. J. Differences in nucleation behavior underlie the contrasting aggregation kinetics of the Aβ40 and Aβ42 peptides. *Proc. Natl. Acad. Sci. U.S.A.* **2014**, *111*, 9384−9389.
(24) Meisl, G.; Kirkegaard, J. B.; Arosio, P.; Michaels, T. C.; Vendruscolo, M.; Dobson, M.; Linse, S.; Knowles, T. P. J. Molecular mechanisms of protein aggregation from global fitting of kinetic models. *Nat. Protoc.* **2016**, *11*, 252−272.
(25) Michaels, T. C. T.; Saric, A.; Habchi, J.; Chia, S.; Meisl, G.; Vendruscolo; Dobson, C. M.; Knowles, T. P. J. Chemical kinetics for bridging molecular mechanisms and macroscopic measurement of amyloid fibril formation. *Annu. Rev. Phys. Chem.* **2018**, *69*, 273−298.
(26) Burgold, S.; Filser, S.; Dorostkar, M. M.; Schmidt, B.; Herms, J. In vivo imaging reveals sigmoidal growth kinetic of amyloid plaques. *Acta Neuropathol. Commun.* **2014**, *2*, No. 30.
(27) Rial, D.; Vázquez, J. A.; Murado, M. A. Effects of three heavy metals on the bacteria growth kinetics: a bivariate model for toxicological assessment. *Appl. Microbiol Biotechnol.* **2011**, *90*, 1095−1109.
(28) Peppas, N. A.; Narasimhan, B. Mathematical models in drug delivery: How modeling has shaped the way we design new drug delivery systems. *J. Controlled Release* **2014**, *190*, 75−81.
(29) Vázquez, J. A. Modeling of chemical inhibition from amyloid protein aggregation kinetics. *BMC Pharmacol. Toxicol.* **2014**, *15*, No. 9.
(30) Landau, M.; Sawaya, M. R.; Faull, K. F.; Laganowsky, A.; Jiang, J.; Sievers, S. A. Towards a pharmacophore for amyloid. *PLoS Biol.* **2011**, *9*, No. e1001080.
(31) Tin, G.; Mohamed, T.; Gondora, N.; Beazely, M. A.; Rao, P. P. N. Tricyclic phenothiazine and phenoselenazine derivatives as potential multi-targeting agents to treat Alzheimer's disease. *MedChemComm* **2015**, *6*, 1930−1941.
(32) Hudson, S. A.; Ecroyd, H.; Kee, T. W.; Carver, J. A. The thioflavin T fluorescence assay for amyloid fibril detection can be biased by the presence of exogenous compounds. *FEBS J.* **2009**, *276*, 5960−5972.
(33) Yang, F.; Lim, G. P.; Begum, A. N.; Ubeda, O. J.; Simmons, M. R.; Ambegaokar, S. S.; Chen, P. P.; Kayed, R.; Glabe, C. G.; Frautschy, S. A.; Cole, G. M. Curcumin inhibits formation of amyloid beta oligomers and fibrils, binds plaques, and reduces amyloid in vivo. *J. Biol. Chem.* **2005**, *280*, 5892−5901.
(34) Jang, M. H.; Piao, X. L.; Kim, J. M.; Kwon, S. W.; Park, J. H. Inhibition of cholinesterase and amyloid-beta aggregation by resveratrol oligomers from Vitis amurensis. *Phytother. Res.* **2008**, *22*, 544−549.
(35) Feng, Y.; Wang, X. P.; Yang, S. G.; Wang, Y. J.; Zhang, X.; Du, X. T.; Sun, X. X.; Zhao, M.; Huang, L.; Liu, R. T. Resveratrol inhibits beta-amyloid oligomeric cytotoxicity but does not prevent oligomer formation. *Neurotoxicology* **2009**, *30*, 986−995.
(36) Lloret-Villas, A. L.; Varusai, T. M.; Juty, N.; Laibe, C.; NovEre, N. Le.; Hermjakob, H.; Chelliah, V. The impact of mathematical modeling in understanding the mechanisms underlying neuro-degeneration: evolving dimensions and future directions. *CPT: Pharmacometrics Syst. Pharmacol.* **2017**, *6*, 73−86.

https://doi.org/10.1021/acsomega.1c00610
ACS Omega 2021, 6, 8680−8686